

Light-Driven Semiconductor-Based Micro/Nanomotors

Subjects: Others

Contributor: Vanessa R. A. Ferreira, Manuel A. Azenha

Micro/nanomotors represent a burgeoning field of research featuring small devices capable of autonomous movement in liquid environments through catalytic reactions and/or external stimuli.

Keywords: light-driven motors ; semiconductor ; self-propulsion ; photocatalysis

1. Introduction

Micro/nanomotors are small devices capable of moving autonomously in a liquid medium using catalytic reactions or an external stimulus (chemical fuels, magnetic, ultrasound, or light). The main features generating the movement of these motors are morphological asymmetry (generally created by the deposition of metals on one side of the motors, creating two distinct hemispheres) and the consumption of chemical fuels, as presented later in more detail. Such small automotive devices were recognized for performing sophisticated tasks while moving in different liquid media, which allows them to be applied in the most diverse areas, namely detection, biomedicine, and environmental remediation ^[1]. This versatility has made these micro/nanomotors one of the most promising research topics worldwide.

Regarding the energy source used to generate propulsion, studies on micro/nanomotors can be grouped into five categories corresponding to the type of energy involved: chemical fuels ^{[2][3]}, magnetic fields ^{[4][5]}, electric fields ^[6], acoustic ^[7], and light ^{[8][9]}. Motors powered by chemical fuels often form bubbles or chemical gradients to move. The main challenge in this type of motor is movement control and toxicity. Considering that the chemical fuel most described in the literature is hydrogen peroxide (H_2O_2), the intrinsic toxicity may limit the applicability of these catalytic micro/nanomotors in the biomedical field. In this case, H_2O_2 can be catalytically decomposed into O_2 and H_2O molecules on the surface of micro/nanomotors, creating a chemical gradient that triggers uncontrolled autonomous movement. Ultrasonication, a recently tested energy source, provides robust propulsion but requires more sophisticated equipment. Magnetic motors have their movement controlled under adjusted magnetic fields, which limit their application to specific functions. Electric motors follow electrical gradients, limiting themselves mainly to two-dimensional movements. Motors powered by light, especially solar, have gained prominence due to their advantages, such as their low cost, ease of control, and ability to carry out complex tasks. Light, an abundant, remotely propagated, clean, and controllable energy source, is a promising option for driving micro/nanomotors ^[10]. The most recent reviews describing the main advances in the propulsion conditions of light-driven micro/nanomotors ^{[9][11]} or light-powered micro/nanomachines without the use of chemical fuel ^[8] to make the process greener and expand possible applications date back to 2018.

Propulsion Mechanisms

For a better understanding of the subsequent sections, it is important to make a summary of the different propulsion mechanisms already described in the literature for light-driven micro/nanomotors.

Small devices moving through a fluid face a challenge due to their limited motion at a low Reynolds number ^[12]; that is, they encounter a powerful viscous force. Scientists are working on various methods to tackle this issue and enhance the devices' controlled movement, countering the random Brownian motion that typically hinders them, as shown in **Figure 1**.

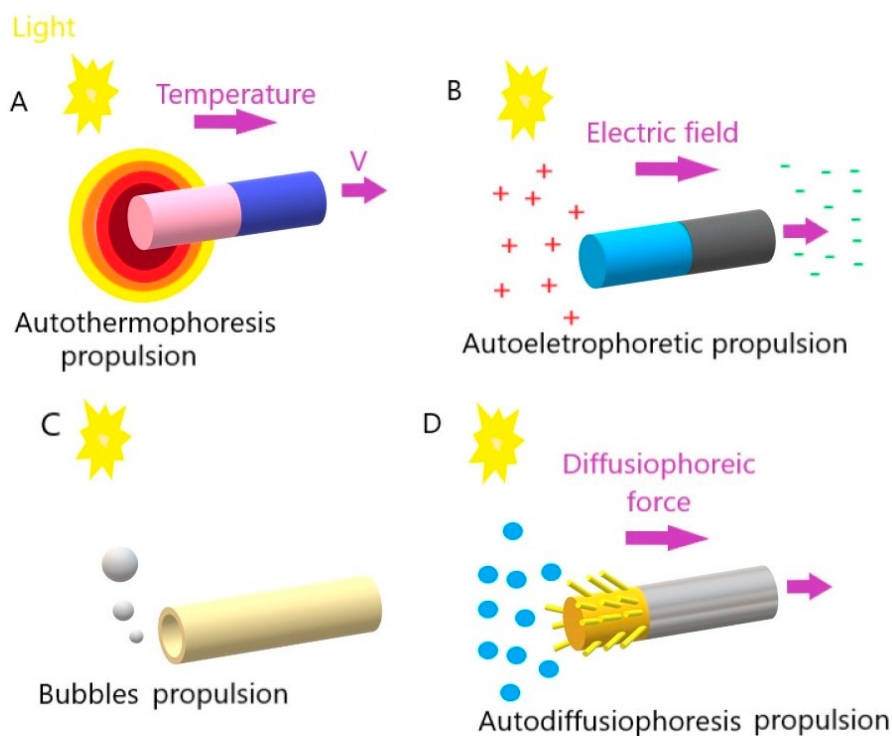


Figure 1. Movement mechanisms of light-driven micro/nanomotors: (A) autothermophoresis, (B) autoelectrophoresis, (C) bubbles, and (D) autodiffusiophoresis.

In photothermal propulsion, the thermophoretic force resulting from the temperature gradient drives the motor as the temperature decreases. When light intensity increases, it generally generates more heat. This increase in temperature creates a thermal gradient, that is, a temperature difference between the hottest and coldest regions. The micro/nanomotors are designed to respond to these temperature changes, as they are made of heat-sensitive materials that expand or contract with temperature variations. When there is a more significant thermal gradient (due to a higher light intensity), the response of these materials is more pronounced. This change in the shape or volume of heat-sensitive materials generates an acting force on the micro/nanomotors, causing them to move or perform some specific action. Thus, in short, temperature controls the speed of these motors through its effect on heat-sensitive materials, influencing the actuation force they generate.

For example, Yang et al. described the propulsion mechanism of micro/nanomotors irradiated with a near-infrared (NIR) light source, in which the absorbed electromagnetic energy was dissipated with heat. Then, a thermal gradient was formed around the surrounding liquid [13]. This increase in temperature gradient resulted in movement by the autothermophoresis of the photothermal materials. This way, it was possible to control the motors' movement through the illumination intensity of the NIR laser. Greater light intensity led to a more significant temperature gradient, resulting in a greater actuation force of the micro/nanomotors.

In auto-electrophoretic propulsion, light plays a crucial role in generating an electric field that, in turn, drives micro- or nano-sized particles. This phenomenon is based on the principles of electrophoresis, which is the movement of charged particles in response to an electric field. In other words, light falls on the particles, activating specific properties that make them electrically charged. The presence of the same light creates an electric field around the charged particles due to electrophoretic interactions. The local electric field results from the asymmetric distribution of charged ions, which are generated from photocatalytic reactions on the surface of micro/nanomotors, specifically on the surfaces of different types of materials. As the electric field is generated under light irradiation, the charged micro/nanomotors are caused to move in response to the area [14][15]. In short, light acts as the trigger to generate electrical charges on particles, and the interaction of these charges with the light-induced electric field results in particle movement. However, it should be noted that depending on the properties of specific materials, such as the metals and semiconductors used to prepare light-driven micro/nanomotors, the type of reaction triggered by the incidence of light can be differentiated. This approach is explored in several applications, such as manufacturing light-driven micro/nanomotors for transporting cargo on a microscopic scale.

In bubble-induced propulsion, the force generated by the bubbles drives the motors in an opposite direction. In this case, light plays a key role in generating and manipulating gas bubbles. Light falls on a light-sensitive material, such as a photocatalyst, and the light-sensitive material undergoes photolysis (the process in which light breaks down precursor molecules, releasing gas (such as oxygen or hydrogen) as a byproduct). The released gas accumulates on the surface of

the micromotor, forming bubbles. The accumulation of bubbles creates a pressure difference on the surface of the micromotor. This results in the expulsion of the bubbles, creating an impulse that drives the micromotor in the opposite direction.

In other words, as bubbles are released from the surface of the motors, resulting from the mostly redox reactions that occur, this unleashes a driving force away from the surface of the motors [16][17]. It is essential to highlight that in these cases, the driving force is assumed to be balanced with the viscous drag force if the vertical forces are ignored.

Finally, in auto-diffusiophoretic propulsion (also named osmotic propulsion), light is crucial in creating chemical gradients that lead to particle movement. The light falls on the surface of the particles, activating specific chemical reactions or surface interactions that change the local chemical composition. As a result of irradiation, a local chemical change occurs that leads to the formation of concentration gradients of certain substances around the particles. The resulting concentration gradients induce a directional movement of the particles, known as diffusiophoresis. This movement occurs due to diffusion forces arising when particles move toward lower- or higher-concentration regions. The directional movement of particles, induced by diffusiophoresis, results in autodiffusiophoretic propulsion.

In short, light creates chemical gradients around particles, triggering directional movement based on diffusion forces. This phenomenon is especially exploited in micromotors and micro/nanometer-scale particles to achieve controlled propulsion in liquid environments [18][19].

There are other movement mechanisms, less described in the LDSM literature, namely photoinduced deformation propulsion, which refers to a propulsion method occurring through shape change (bending, expanding, or contracting) activated by light (photoinduced). This mechanism is particularly associated with photoactive polymeric materials [20] and liquid crystals [21][22] and may also be referenced in metallic compounds that possess properties changing according to the specific light incidence (in terms of intensity, polarization, or frequency). In the case of LDSM, this movement mechanism can be associated with LDSM hybrids with polymers [23]. Light-induced surface tension variation is another movement mechanism that exploits the ability to alter the surface tension of liquids through exposure to light, in order to generate movement and force on LDSM. In this case, a semiconductor with chemical or physical properties altered by light exposure can directly affect the surface tension of the surrounding liquid, resulting in its movement [24]. Another example is localized light exposure, which can create gradients of surface tension, with areas of higher and lower tension. These gradients can induce liquid flows or move LDSM placed on the liquid surface, exploiting the phenomenon known as the Marangoni effect, where the liquid flows from areas of low surface tension to areas of high surface tension [25][26].

2. Light-Driven Semiconductor-Based Micro/Nanomotors

LDSM are mobile devices created from materials that conduct electricity activated by light, as is the case with some metal oxides (i.e., TiO_2 , ZnO , CuO_2 , BiVO_4 , WO_3) [9]. Materials, in general, have two energy bands: the valence band (highest occupied) and the conduction band (lowest unoccupied), separated by an interval called band gap (E_g) that defines electrical conductivity. Non-conducting materials have a large E_g (≥ 4 eV), which limits electron transfer. Semiconductors have intermediate conductivity (E_g between 1 and 4 eV), and the higher the E_g value, the lower the range of radiation wavelengths capable of triggering propulsion. In other words, the higher the E_g , the lower the visible (Vis) light absorption capacity of the semiconductor. The compilation of recent data from the literature, presented in **Table 1**, shows that to produce LDSM, materials with photocatalytic activity, namely metal oxides (highlighting TiO_2 , CuO_2 , and ZnO), are mainly used in these materials. These are chosen because they can utilize energy from external light sources and surrounding chemicals to achieve efficient propulsion. Its photocatalytic properties convert optical and chemical energy into mechanical movement through photocatalytic reactions, making it possible to obtain motors with propulsion modulation through chemical concentration or light intensity. In other words, micro/nanomotors based on photocatalytic semiconductors can have controlled propulsion, for example, by simply regulating the intensity of the light source with on/off tests (turning on the irradiation source, letting it reach the maximum speed and turning off the source), or even by the position of the irradiation beam. Furthermore, they can operate with low optical and chemical energy input, making them ideal for industrial applications. Another important factor to consider in this type of motor is the production of free radicals during photocatalytic reactions that offer the potential for environmental remediation, especially in the degradation of organic pollutants, since the gradient or asymmetric distribution of photocatalytic products generated by photocatalysts when exposed to the light of a specific wavelength (such as ions, molecules or gases), trigger cycles of redox reactions with the surrounding reactants that interfere with propulsion, which may or may not be beneficial.

Table 1. Compilation of recent literature data on the production and performance of LDSM.

Chemical Composition	Propulsion Mechanism	Morphology	Scale (nm)	Light Range and Maximum Intensity (mW.cm ⁻²)	Velocity [$\mu\text{m}\cdot\text{s}^{-1}$]	Ref.
TiO ₂ /Au motors	Self-electrophoretic	Janus hollow sphere	~800	UV (16)	48.5	[27]
TiO ₂ -Fe motors	Self-electrophoresis	Janus sphere	~2000	UV (21)	7.8	[28]
TiO ₂ @N-Au motors	Self-electrophoresis	Wire	235 ± 35	Vis (100)	2.5 ± 0.4	[29]
TiO ₂ -Au motors	Self-electrophoresis and acoustic effect	Capsule	~2150	UV (80)	39.5	[30]
2D TiO ₂ motors	Bubble-propelled	Tubes	150	UV (50)	52.0	[17]
Au/TiO ₂ motors	Self-electrophoresis	Capsule	175	Vis (100)	1.9 ± 0.5	[31]
Hybrid TiO ₂ /Au/Pt motor	Self-diffusiophoresis	Janus sphere	~1000	UV (10)	13.0	[18]
Cubes Co ₃ O ₄ @TiO ₂ and Platelets Co ₃ O ₄ @TiO ₂	Brownian diffusion and self-electrophoresis	Janus sphere	900	UV (20) Vis (16)	Cubes—5.0 and 10.0 Platelets—13.9 and 19.3 for Vis and UV light	[32]
Au/TiO ₂ motors	Self-diffusiophoresis	Pillars	1500	UV (320)	4.0	[19]
Hydrogel-based motors	Bubble-propelled	Spheres	200–370	UV (300)	100.0 to 135.0	[33]
Hybrid TiO ₂ @SiO ₂ motors	Self-diffusiophoresis	Janus spheres elongated	3200	UV (20)	5.0 ± 2.0	[34]
Hybrid light/acoustic-powered motors	Self-diffusiophoresis	Janus spheres elongated	1500	UV (50)	27.0 ± 9.0	[35]
Cu@TiO ₂ and Au@TiO ₂ motors	Self-electrophoresis and diffusiophoresis	Janus spheres	700	UV (315)	Au = 23.0 Cu = 38.0	[36]
Au@TiO ₂ -SiO ₂ motors	Self-electrophoresis	Janus spheres elongated	250	NIR (10)	0.7 ± 0.1	[37]

Chemical Composition	Propulsion Mechanism	Morphology	Scale (nm)	Light Range and Maximum Intensity (mW.cm ⁻²)	Velocity [$\mu\text{m}\cdot\text{s}^{-1}$]	Ref.
<i>TiO₂/Pt; SiO₂/Pt ZnO/Pt motors</i>	Self-electrophoresis	Janus spheres	~3000	NIR (10)	21.0 to 30.0	[38]
Magnetic CoO–TiO ₂ motors	Self-electrophoresis	Janus sphere	~4000	UV (100) Vis (6)	Vis = 11.5 ± 0.7 UV = 6.2 ± 0.2	[39]
TiO ₂ /MnO ₂ motors	Bubble-propelled	Janus sphere	240	UV (20)	48.1	[16]
Metal/TiO ₂ motors ((Pt, Au, Ag, Fe, Cu)	Self-electrophoresis	Janus sphere	2200	UV (40)	Pt = 8.9; Au = 2.1 Ag = 3.6; Fe = 4.3 Cu = 5.1	[40]
TiO ₂ –Pt motors	Self-electrophoresis	Janus sphere	1200	UV (123)	35.0	[41]
TiO ₂ motors	Self-electrophoresis	Hollow spheres	~1000	UV–LED (590)	6.5 to 9.5	[42]
Au/TiO ₂ /Cu ₂ O hybrid motors	Self-electrophoresis and diffusiophoresis	Spheres elongated	~5000	UV–Vis (600)	Value not calculated	[43]
dielectric SiO ₂ /TiO ₂ motors	Self-electrophoresis	Spheres	~1000	UV (35)	8.6	[15]
MOFs funcionalizado	Self-electrophoresis	Spheres elongated	2600	UV–Vis (14)	40.0	[44]
Au–ZnO motors	Self-electrophoresis	Rods	90	UV (250)	24.2	[45]
ZnO/Pt motors	Self-electrophoresis	Janus spheres	~2000	UV (135)	32.0	[46]
Sb ₂ Se ₃ /ZnO motors	Self-electrophoresis	Wire	100	UV (200)	3.9	[47]
ZnO/ZnO ₂ /Pt motor	Self- diffusiophoresis and bubble-propelled	Janus spheres	5000	Vis (20)	352.0	[48]

Chemical Composition	Propulsion Mechanism	Morphology	Scale (nm)	Light Range and Maximum Intensity (mW.cm ⁻²)	Velocity [$\mu\text{m}\cdot\text{s}^{-1}$]	Ref.
Au/ Fe ₃ O ₄ motors	Self-electrophoresis and diffusiophoresis	Rods	200	Vis (33)	37.2	[49]
ZnO/Pt motors	Self-electrophoresis diffusiophoresis	Sheets	~1000	UV (400)	2.5	[50]
Graphene Aerogel motors	Self-electrophoresis	Janus spheres	100–1000	NIR (9)	17.6	[51]
GQDs/PtNPs motors	Self-diffusiophoretic	Tubs	nano	Vis (N/A)	440.0	[52]
Cu ₂ O@GO motors	Self-electrophoresis/ diffusiophoretic and thermophoresis	Spheres	~2000	Vis (32) NIR (2.5)	16.6	[13]
Cu ₂₊₁ O motors	Self-diffusiophoretic	Spheres	~1000	Vis (84)	107.0	[53]
Cu ₂ O@CdSe motors	Self-diffusiophoretic	Octahedral structure	~1000	UV–Vis (180)	55.1	[54]
Cu ₂ O motors	Self-diffusiophoretic	Octahedral structure	864	UV–Vis (180)	10.8	[55]
GO/BiVO ₄ motors	Self-diffusiophoretic	Spheres	micro	Vis (180)	25	[56]
Single-component BiVO ₄ motors	Self-diffusiophoretic	Janus star	4000–8000	UV–Vis (5)	5 ± 1	[57]
TiO ₂ /Pt motors	Self-electrophoresis	Janus sphere	~1 μm	UV (40)	9.7 ± 1.98	[58]
Au-Cu motors	Bubble-propelled	Tubes	~1 μm	NIR (6.4)	2.2 ± 0.3	[59]
TiO ₂ crystalline motors	Self-electrophoresis/ diffusiophoretic	Janus sphere	500 nm	UV (80)	11	[60]
WO ₃ motors	Self-diffusiophoretic	Spheres	1-2 μm	UV (160)	2.0 ± 0.1	[61]

N/A—Not applicable.

Table 1 presents a selection of the articles published in the past 5 years (2018–2023) on LDSM having, in the researchers' view, the most significant implications on the optimization of light-driven movement. This table shows the main factors to consider for a more efficient and controlled propulsion speed: chemical constitution, morphology, scale,

mechanisms of action, light source, and respective intensity. For each study, optimized movement speeds were presented to facilitate comparison.

2.1. Semiconductors Most Used in the Preparation of Light-Driven Micro/Nanomotors

As previously mentioned, and corroborated by **Table 1**, the semiconductors most used to prepare LDSM are metal oxides with photocatalytic activity and some carbon sources. In the following sub-sections, the semiconductors most used for preparing LDSM will be presented. After a summary of the previous state of the art, innovative and representative examples of the advances achieved in the past 5 years are presented.

2.1.1. Light-Driven TiO₂-Based Micro/Nanomotors

TiO₂ has always been the most used semiconductor metal oxide to produce LDSM, due to its photocatalytic characteristics associated with chemical stability under light irradiation, low cost, and low toxicity [9]. Light-driven TiO₂ micro/nanomotors have been widely reported, considering the high applicability of this semiconductor in photocatalysis. With TiO₂ being the semiconductor most used to produce photocatalysts and LDSM being sophisticated versions of photocatalysts, extensive use of TiO₂ in the production of LDSM is expected. The first example of TiO₂-based micromotor systems was reported in 2010 by Sen and collaborators [62]. Since then, several studies have been reported with TiO₂-based micro/nanomotors [15][16][18][28][31][33][36][39][41][42][43][63][64]. Many parameters have been scrutinized in recent years to prepare more efficient TiO₂-based micromotors, namely the morphology, scale, and degree of crystallinity of the semiconductor. The spherical and tubular shape on the micrometric scale has been more widely described in the literature due to the simplicity of the synthesis methods, as well as the reproducibility and controllability of other important parameters [11]. However, in the recent past, attempts have been made to reduce the scale, a slow process considering the difficulty inherent in the reproducibility of the synthesis process. The structure asymmetry is one of the most discussed parameters for obtaining propulsion for light-driven TiO₂-based motors.

The agglomeration effects and propulsion conditioned by the interaction between motors were explored and often avoided through the crystallinity of the semiconductor [27]. The different degrees of crystallinity, easily obtained with this type of semiconductor (anatase and rutile), are also the subject of extensive study, considering the importance of this parameter for optimizing the photocatalytic process and consequent acceleration of the propulsion mode. The anatase phase of TiO₂ has generally been considered the most effective crystalline phase for obtaining TiO₂-based micro/nanomotors with an improved photocatalytic activity, resulting in faster movement. In other words, the main motivation in the study and development of this type of motor, until 2016, was to understand the propulsion mechanism inherent to the different morphologies and ways of optimizing the same mechanism to accelerate the light-driven movement. More recently, in addition to improved propulsion speed and testing less dense structures [27], the focus has been on overcoming one of the significant limitations of the use of TiO₂ in LDSM, the high value of E_g (~3 eV), which restricts the activation of TiO₂-based micromotors upon UV light irradiation (≤ 390 nm). Different strategies have been explored, in the past few years, to expand the light-absorption capabilities of TiO₂-based micromotors to the visible region, i.e., a combination of TiO₂ with a Vis-light-absorbing photocatalyst by a p-n junction [32][39][43], surface doping [29][31], dye sensitization [65], or reducing TiO₂ to black TiO₂ [66]. Gibbs and collaborators [43] recently explored joining two photocatalytic semiconductors, TiO₂ and CuO₂, to prepare hybrid micromotors. In this study, a p-type semiconductor (the dominant charge carriers are positive "holes") such as CuO₂ was conjugated with an n-type semiconductor (in which the dominant charge carriers are electrons) such as TiO₂ to modify the electrical conductivity of the hybrid photocatalyst. These micromotors were produced by electron beam evaporation, using SiO₂ microspheres as a support. Initially, TiO₂ was deposited at an oblique angle on SiO₂, then the sample stage was rotated by 180°, and Cu was deposited on the "tail" of TiO₂, generating chevron-shaped morphologies. These hybrid micromotors showed self-propulsion in water under UV and Vis irradiation (380–450 nm), through translational and rotational movements, respectively. The use of the n-type semiconductor (TiO₂) resulted in the introduction of a small amount of an impurity into the CuO₂ crystalline structure that modified its electronic properties, giving rise to additional energy states in the band gap, which thus reduced the band gap. A potential barrier is formed at the interface of the CuO₂ (p-type semiconductor) and TiO₂ (n-type semiconductor) junction, creating an internal electric field. This interface acts as a barrier to prevent e^-/h^+ recombination, one of the strategies to increase the photocatalytic efficiency of TiO₂-based motors. This strategy, in addition to being able to be applied to other semiconductors, such as ZnO, has the advantage of being a more economical approach since noble metals, widely used in the production of efficient micromotors [9], are not necessary for this approach.

Sensitization with organic dyes of Si/TiO₂ nanotrees was demonstrated by Zheng et al. [65] to obtain Vis-light-driven nanomotors. In this study, dyes with a different sensitivity to Vis light (green, red, and blue) were incorporated into the surface of the Si/TiO₂ nanotree to control the nanomotors' movement depending on the source of irradiated light. The method of producing large-scale nanotree structures was based on a modified metal-assisted chemical etching process.

This was followed by the hydrothermal growth of the TiO₂ nanowires. Before the dye adsorption step, the Janus TiO₂/Si nanotree forest was heat treated in air at 450 °C for 30 min. For sensitization, three different dyes were used—N719, D5, and SQ2. The prepared nanotree forests were stained by immersion in an ethanolic dye solution, for incorporation of the dyes, each with a Vis light absorption capacity in a particular range. Thus, when blue or red Vis light is applied, the groups of Si/TiO₂ nanomotors with SQ2 and D5, respectively, will be activated and presented with a movement controlled by the action of the corresponding light source.

The reduction of TiO₂ to its black form is a method that can decrease the bandgap energy. Black TiO₂ can be obtained through thermal treatment (temperature ramps up to approximately 400 °C) in controlled environments, such as reducing atmospheres (e.g., nitrogen atmosphere) or under vacuum conditions. This process can induce changes in the crystal structure that can involving the introduction of defects, such as oxygen vacancies, interstitial defects, and structural disorder, thereby creating additional electronic states within the bandgap and reducing the bandgap energy.

Consequently, electrons can be excited by lower-energy photons, such as those from visible light, thereby increasing the absorption efficiency of TiO₂ in this region of the electromagnetic spectrum. The utilization of black TiO₂ to create LDSM based on TiO₂ with propulsion driven by visible light has been discussed in the literature as a beneficial alternative for achieving solar-light-driven self-propulsion, particularly suitable for biomedical applications [66].

The nanomotors, specifically SQ2 (red) and D5 (blue), exhibited spontaneous trajectories forming the letters 'r' and 'b' as they navigated under the influence of blue and red light, respectively. This happened because the red illuminations (660 nm) were constant in terms of position and irradiation intensity, while the 475 nm blue illuminations were lit sequentially from various directions to rotate the sensitized micromotor contained the D5 dye, regardless of the direction of the red illumination. During this process, the orientation of the SQ2-loaded micromotor was locked by the illumination direction of the 660 nm red light and did not show any rotation with the blue light source. Comparatively, fixed blue 475 nm illumination with rotating red 660 nm illumination only drove the rotation of the sensitized micromotor SQ2 without affecting the alignment of the sensitized micromotor D5. This study demonstrated that dye-sensitized micromotors could indeed be controlled independently.

Therefore, this work had a double importance, considering obtaining a propulsion response driven by Vis light and the possibility of obtaining independent movement for each nanomotor to create an essential cooperative action for different applications, particularly in biomedicine.

2.1.2. Light-Driven ZnO-Based Micro/Nanomotors

ZnO also stands out as a semiconductor with auspicious photocatalytic properties, boosted by its non-toxicity, high electron mobility, and an $E_g \sim 3.37$ eV. This characteristic gives ZnO a wide range of radiation absorption and high photostability, in addition to being a semiconductor that easily converts light energy into kinetic energy to drive motors. Furthermore, ZnO is known to have a high electron and hole mobility, which may contribute to a faster response to light stimuli. However, despite these advantages, its application in motor research is limited due to its high density and low colloidal stability. Even so, ZnO-based photocatalytic materials have been recognized as promising agents in the photocatalysis of environmental pollutants, with potential applications in light-driven micro/nanomotors.

The compilation of different studies carried out until 2018 with light-driven ZnO-based micro/nanomotors described several applications and developed different key points that include propulsion mechanisms, energy efficiency, and possible biomedical applications. Many studies have explored different propulsion mechanisms for ZnO-based micromotors, such as the release of oxygen bubbles or the generation of electrochemical currents under the influence of light, to make these motors faster.

There was an emphasis on optimizing energy efficiency, trying to maximize the conversion of light energy into the efficient movement of micromotors.

In the past 5 years, the focus in the study of ZnO LDSM has continued to be the optimization of the propulsion mechanism to accelerate the movement, but also the concern of its the directional control [45][46][47][48][50][67]. The ability to control light-driven ZnO-based micro/nanomotors remotely by playing with the positioning and intensity of the light source has been widely studied, aiming at the development of precise control systems. Combined with this, the exploration of the nanometer scale proved to be effective in improving propulsion both in speed and direction control. An example of this was the study of light-driven Au–ZnO nanorod motors developed using hydrothermal methods to remove antibiotics from aquatic environments [45]. This study considered different parameters, such as the size and diameter of the nanorods, to obtain nanomotors with controlled and efficient propulsion. The 0.85 ± 0.16 μm size combined with a diameter of 90 ± 24

nm were considered ideal parameters for improved movement. UV light intensity was also considered for propulsion control purposes. With on/off tests, it was possible to verify that when the light was turned off, the speed of the nanomotors gradually decreased from $24 \pm 4 \mu\text{m}\cdot\text{s}^{-1}$ to Brownian motion. The presence of Au allowed the optimization of the separation of charges on the nanorods' surface, positively affecting both the self-propulsion and the photocatalytic degradation performance of tetracycline.

The study of the size of ZnO/Pt Janus motors (1.5 to 5 μm) showed a notable difference in light-driven speed resulting from different propulsion mechanisms due to different porosity scales. In other words, the smaller micromotors (1.5 μm) exhibited self-diffusiophoresis due to their microporous structure, obtained through the catalytic decomposition of H_2O_2 inside the particle. The rapid propulsion observed in the 5 μm micromotors was attributed to the mesoporous interface structure, leading to efficient bubble nucleation and expulsion through the generation of small, high-density microbubbles. The impressive bubble propulsion speed exhibited by the mesoporous ZnO/Pt micromotors set a new standard when compared to previously reported Janus micromotors utilizing non-heavy materials such as PS and silica. In this way, it was possible to obtain a very fast micromotor ($350 \mu\text{m}\cdot\text{s}^{-1}$) by adjusting the diameter of the Janus structure to 5 μm , representing a double acceleration compared to smaller micromotors [48].

Integration with other materials, especially through hybridization with other semiconductors, has also been highlighted in recent years, considering the need to overcome some limitations inherent to semiconductors in their individual state, through synergistic and/or cumulative effects. Some studies have explored the integration of ZnO with other materials to further improve the performance of micromotors. For example, Zhang and collaborators presented core-shell nanomotors utilizing Sb_2Se_3 nanowires as the core [47]. These nanowires were prepared via the physical vapor deposition method, with a polycrystalline ZnO shell (150 nm) applied to the Sb_2Se_3 nanowire through atomic layer deposition. The ZnO shell functions as a charge collector for both Sb_2Se_3 nanowire photovoltaics and nanomotors. This study showcased a breakthrough in micromotor navigation. A significantly faster and more precisely targeted navigation of the general micromotor was achieved through the strategic assembly of two cross-aligned nanomotors and the application of polarized light. This investigation focused on the polarization state of light, exploiting the anisotropic crystalline structure of the motor that facilitated the preferential adsorption of polarized light parallel to the Sb_2Se_3 nanowires.

As a result, the $\text{Sb}_2\text{Se}_3/\text{ZnO}$ core-shell nanomotor exhibited robust dichroic swimming behavior, displaying a movement speed three times faster when illuminated with parallel polarized light compared to perpendicular polarized light. Moreover, incorporating two cross-aligned dichroic nanomotors led to the development of polarotactic nanomotors, endowed with the ability to control the movement direction based on the polarization of the incident light. This advancement not only enhances the speed and precision of micromotor navigation but also opens up possibilities for applications where directional control is crucial.

2.1.3. Light-Driven CuO_2 -Based Micro/Nanomotors

CuO_2 is also one of the photocatalytic semiconductors used for the production of light-driven micro/nanomotors, mainly due to the reduced E_g (approximately 0.75 eV) that makes the motors based on CuO_2 Vis-light-responsive. The high surface area that increases the adsorptive capacity of these micro/nanomotors is also an important characteristic of this semiconductor.

Research into light-driven micromotors using CuO_2 has been and continues to be less common than that using materials such as ZnO or TiO_2 . However, in general, the few publications that have been presented on light-driven CuO_2 -based motors have focused on optimizing the efficiency of converting light energy into efficient propulsion in specific applications such as biosensing and drug delivery [40], through tests with structures with different morphologies and sizes.

In the past 5 years, the number of publications on light-driven CuO_2 -based motors has increased, with the main objective of optimizing the process of converting light energy into movement. The main novelty involves the optimization of surface characteristics related to the crystalline state of the semiconductor and the capability to manipulate different crystalline facets on the surface of the same LDSM [53][54][55][60][67]. For example, using CuO_2 as a semiconductor associated with asymmetric structures with specific geometry was one of the strategies described to achieve Vis-light-driven micro/nanomotors [55]. In this study, the authors considered CuO_2 to prepare the micro/nanomotors because it is a semiconductor with a high surface area, responsive to Vis light irradiation, and with different crystalline phases that can enhance self-propulsion. The previous characteristics were combined with a truncated octahedron morphology that allowed the preservation of the controllable crystalline facets {100} and {111} in a single colloid. These morphological and crystallinity characteristics are essential to achieve directed and efficient propulsion. These parameters will be covered in greater detail in the following sections. In this case, it is necessary to highlight the relevant choice of CuO_2 as a base material, which combined all these essential characteristics to prepare highly efficient Vis-light-driven micro/nanomotors.

Another work was described on Vis-light-driven micro/nanomotors based on CuO_2 , and in this case, the choice of semiconductor was made considering the possibility of introducing oxygen-vacancy-based Cu_{2+1}O to improve the self-propulsion of the micro/nanomotors [53]. Oxygen vacancies are crystalline defects that trap photogenerated electrons, increasing the materials' photocatalytic activity. These motors can be synthesized in a single step, with low costs and without additional modifications. Cu_{2+1}O micro/nanomotors demonstrate excellent propulsion on biocompatible fuels such as tannic acid. These motors reached maximum speeds of up to $18 \mu\text{m}\cdot\text{s}^{-1}$ in pure water under Vis light, comparable to conventional Pt-based catalytic micromotors powered by toxic H_2O_2 [68].

2.1.4. Hybrid Light-Driven Semiconductor-Based Micro/Nanomotors

The mixture of two or more semiconductors in the same LDSM has the advantage of reconciling and/or creating synergistic effects between the main characteristics of each semiconductor, as well as overcoming some of the limitations of each semiconductor in its individual state. Since work with LDSM began, one of the limitations most mentioned by researchers has been the limited charge separation for light-driven micromotors of single-component semiconductors, which leads to weak propulsion power and low motion. Therefore, it is important to construct hybrid structures to increase the photocatalytic performance, improve the motor motility, and satisfy the demand for practical applications.

Chen et al. described the production of Vis-light-driven $\text{Cu}_2\text{O}@ \text{CdSe}$ micromotors with excellent cationic dye removal capabilities [54]. The gap between the Cu_2O and CdSe semiconductors formed a heterojunction that effectively inhibited the recombination of photogenerated e^-/h^+ pairs and improved the photocatalytic activity and, consequently, the propulsion speed of the $\text{Cu}_2\text{O}@ \text{CdSe}$ micromotors. Self-propulsion reached a maximum speed of $42 \mu\text{m}\cdot\text{s}^{-1}$ in biological environments due to the formation of the asymmetric chemical concentration gradient around the motors. Furthermore, the adsorbent capacity of the $\text{Cu}_2\text{O}@ \text{CdSe}$ micromotors was confirmed with a fast adsorption rate of 96% in methyl blue after 10 min, mainly because of the high surface area of Cu_2O .

Another process for obtaining Vis-light-driven hybrid nanomotors was proposed by Ge and collaborators [46]. This work described new nanomotors that moved in response to Vis light by Janus $\text{TiO}_2/\text{MnO}_2$ nanoparticles and aimed to create cost-effective nanomotors activated by Vis light without needing heavy metals for the required movement asymmetry. The synthesis process was based on the growth of MnO_2 nanoflakes in one of the hemispheres of TiO_2 spheres by the photoreduction of KMnO_4 under aerobic conditions. In this case, propulsion was dependent on the use of H_2O_2 . Considering the catalytic decomposition of H_2O_2 promoted by MnO_2 nanoflakes, the engaging propulsion mechanism generates oxygen bubbles and consequently repels the nanomotors forward in the solution. For this reason, compared to other noble-metal-propelled Janus nanomotors (characterized by a self-electrophoretic propulsion mechanism), $\text{TiO}_2/\text{MnO}_2$ are still weak in propulsion speed ($48 \mu\text{m}\cdot\text{s}^{-1}$). To overcome this limitation, it was proposed to reduce the weight of the nanomotors or prepare a binary composite of a noble metal and MnO_2 to further improve the catalytic performance in the decomposition of H_2O_2 and consequently improve propulsion.

Hybrid light-driven semiconductor-based micro/nanomotors is a recent topic that will certainly be emphasized in the future. The blend involving carbon constituents, specifically graphene, posited as a potential semiconductor, has proven to be a beneficial and exceedingly promising prospect

Light-Driven Graphene-Based Micro/Nanomotors

Graphene has exhibited promise as a semiconductor on a small scale in prior research, but the surge in studies pertaining to its application in LDSM has increased significantly. It is represented by a two-dimensional hybridized sp^2 -carbon sheet with attractive properties, such as a large surface area, good electrical conductivity, high intrinsic mobility, and excellent mechanical resistance [69]. Generally, it is used as a base material where catalyst nanoparticles are distributed asymmetrically to propel the graphene particle [44][52]. Using graphene as the main component provides new possibilities for applying light-driven micro/nanomotors, mainly in biomedicine and environmental remediation. For example, the coupling of graphene to micro/nanomotors makes it possible to create dynamic platforms for water decontamination by increasing the adsorption capacity of organic pollutants [70]. The first studies on light-driven graphene-based motors explored possible combinations of graphene with other materials to optimize the properties of micromotors (generally metal oxides) to increase the efficiency of converting light energy into movement. Another point addressed was modifications to the surface of the graphene-based motors to improve propulsion efficiency or to allow specific functionalization for specific applications. Despite all of this, the number of scientific publications on light-driven micromotors using graphene has been relatively limited, and it has been in the past 5 years that there has been greater interest in this material due to its unique properties [13][51][56].

The main points covered in the recent literature on light-driven graphene oxide (GO)-based micro/nanomotors have included using light to generate temperature gradients on the GO surface, resulting in directional movement [13]. This could involve absorbing light and converting that energy into motion, thus creating photothermal micromotors. For example, Yang and collaborators described the highly efficient light-driven micromotor composed of Cu₂O@GO, capable of being propelled by various biocompatible fuels [13]. By the hybridization of Cu₂O and GO, the micromotors exhibited an enhanced photocatalytic performance, enabling efficient propulsion under Vis and NIR light. Compared to conventional Cu₂O micromotors driven solely by visible light, the Cu₂O@GO micromotors achieved three times faster movement across the entire visible light spectrum when fueled by glucose. Moreover, the motors, benefiting from the enhanced photocatalysis and local photoinduced thermal effects induced by GO, can be powered by near-infrared light using biocompatible fuels like glucose, leucine, and urea solutions, reaching speeds of up to 11 $\mu\text{m}\cdot\text{s}^{-1}$ (for glucose). This innovative approach of improving light-driven micromotor performance through GO doping offers a promising avenue for developing micromotors with potential applications in biological environments.

The general interest in developing and optimizing methods to control graphene-based micromotor direction and speed using different light characteristics, such as intensity or polarization, has continued to be one of the main objects of study in the past 5 years. NIR light-steered graphene aerogel has been described as a promising micromotor with controlled self-propulsion [51]. These micromotors, with a Janus structure, were based on reduced graphene oxide aerogel microspheres (RGOAM) obtained by an electrospray methodology. Using aerogel particles, this methodology made it possible to obtain micromotors with crucial isotropic characteristics, namely low density, which allowed efficient self-propulsion without adding chemical fuels. The low density reduces the resistance to fluids on the water surface, making RGOAM motors faster (up to 18 $\mu\text{m}\cdot\text{s}^{-1}$) than the recent literature has reported. The direction and speed of movement in the water were controlled by the NIR light on/off effect. Considering the high adsorption and charge capacity provided by reduced graphene oxide, these micromotors were successfully applied in the active charge–transport–release of dyes on demand.

Yang et al. described a highly efficient light-driven Cu₂O@GO micromotor that can be propelled by biocompatible fuels such as glucose [13]. In this study, the main objective of using GO was to obtain self-propulsion by Vis and/or NIR light. Compared to conventional Cu₂O micromotors, which can only be driven by Vis light, Cu₂O@GO micromotors showed speeds three times faster (17 $\mu\text{m}\cdot\text{s}^{-1}$) under the same conditions using glucose as fuel. The values were slightly lower than the propulsion speed achieved when using NIR light (11 $\mu\text{m}\cdot\text{s}^{-1}$). Proof of the propulsion by NIR light, although slower, associated with the use of biofuels could be crucial for potential biological applications.

It is important to note that the field of light-driven graphene-based micromotors has evolved rapidly, and a more significant number of publications is expected in the coming years aimed at possible specific applications, mainly in biomedicine. The exploration of other possible applications for these micromotors includes targeted drug delivery or micro/nanometric scale manipulation.

Light-Driven MXene-Based Micro/Nanomotors

Another class of 2D hybrid LDSM has emerged recently, utilizing derivatives of MXenes. MXenes are a group of 2D materials characterized by the general formula M_{n+1}X_nT_x (n = 1, 2, 3), where M represents transition metals such as Ti, X represents C and/or N, and T_x denotes the surface-terminating functionality, which can be -O, -F, or -OH. Their multilayer structure provides a large surface area, making them appealing for the development of new LDSM.

In a pioneering study, sandwich-like structures comprising TiO₂@Ti₃C₂/Pt were created to serve as LDSM [71]. The Ti₃C₂ nanoflakes (derived from exfoliated MXene microparticles) were subjected to a Pt deposition process on one side, which allowed this side to be protected from oxidation while increasing the photocatalytic activity of the new LDSM. Simultaneously, the exposed side of the Ti₃C₂ nanoflakes spontaneously formed a superficial TiO₂ layer through oxidation, triggering enhanced self-propulsion. This study presented an innovative proof of concept for fuel-free LDSM utilizing 2D materials, showcasing enhanced photodegradation capabilities against environmental pollutants.

Another investigation focused on converting Ti₃C₂T_x MXene microparticles into photocatalytic TiO₂ through thermal annealing processes while preserving the distinctive multilayered structure of MXenes. Following Pt layer deposition and surface impregnation with magnetic $\gamma\text{-Fe}_2\text{O}_3$ nanoparticles, the resulting micromotors exhibited enhanced self-propulsion (16 $\mu\text{m}\cdot\text{s}^{-1}$) when exposed to UV light in pure water [72].

Following a similar line of research, Urso et al. [73] explored LDSM based on TiO₂ microparticles derived from MXenes, utilizing Au and Ag, which revealed different electronic properties at the metal–TiO₂ interface. After transforming Ti₃C₂T_x MXene particles into multilayered TiO₂ through thermal annealing, thin layers of Au or Ag were asymmetrically deposited

on their surface via sputtering. The resulting micromotors were tested in pure water with H₂O₂ as fuel. Under UV light, both types of micromotors exhibited self-propulsion, with Au-TiO₂ micromotors demonstrating superior velocities compared to Ag-TiO₂. The higher speed of Au-TiO₂ micromotors was attributed to the stronger built-in electric field at the Au-TiO₂ Schottky junction (a consequence of MXene derivation). This field enhances the separation of photogenerated e⁺/h⁻ pairs in TiO₂ and promotes hole accumulation at the interface. In the presence of H₂O₂, micromotors deposited with different metals present different self-propulsion movements, highlighting the importance of metal-semiconductor interfaces (considering electronic properties) and the impact of the choice of metal on the performance of the micromotor. Au-TiO₂ micromotors showed a slight enhancement in velocity when exposed to UV light, whereas Ag-TiO₂ micromotors exhibited self-propelled motion even without UV light, driven by self-diffusiophoresis. When exposed to UV light, Ag-TiO₂ micromotors demonstrated the highest propulsion speed due to the combined effect of Ag catalytic activity and self-electrophoresis.

References

1. Soto, F.; Karshalev, E.; Zhang, F.; de Avila, B.E.F.; Nourhani, A.; Wang, J. Smart Materials for Microrobots. *Chem. Rev.* 2022, 122, 5365–5403.
2. Somasundar, A.; Sen, A. Chemically Propelled Nano and Micromotors in the Body: Quo Vadis? *Small* 2021, 17, e2007102.
3. Karshalev, E.; de Ávila, B.E.-F.; Wang, J. Micromotors for “Chemistry-on-the-Fly”. *J. Am. Chem. Soc.* 2018, 140, 3810–3820.
4. Büttgenbach, S. Electromagnetic Micromotors—Design, Fabrication and Applications. *Micromachines* 2014, 5, 929–942.
5. Zhou, H.; Mayorga-Martinez, C.C.; Pané, S.; Zhang, L.; Pumera, M. Magnetically Driven Micro and Nanorobots. *Chem. Rev.* 2021, 121, 4999–5041.
6. Wu, Y.; Yakov, S.; Fu, A.; Yossifon, G. A Magnetically and Electrically Powered Hybrid Micromotor in Conductive Solutions: Synergistic Propulsion Effects and Label-Free Cargo Transport and Sensing. *Adv. Sci.* 2023, 10, 202204931.
7. Xiao, Y.; Zhang, J.; Fang, B.; Zhao, X.; Hao, N. Acoustics-Actuated Microrobots. *Micromachines* 2022, 13, 481.
8. Villa, K.; Pumera, M. Fuel-free light-driven micro/nanomachines: Artificial active matter mimicking nature. *Chem. Soc. Rev.* 2019, 48, 4966–4978.
9. Zhan, Z.; Wei, F.; Zheng, J.; Yang, W.; Luo, J.; Yao, L. Recent advances of light-driven micro/nanomotors: Toward powerful thrust and precise control. *Nanotechnol. Rev.* 2018, 6, 383–404.
10. Yuan, K.; Bujalance-Fernández, J.; Jurado-Sánchez, B.; Escarpa, A. Light-driven nanomotors and micromotors: Envisioning new analytical possibilities for bio-sensing. *Microchim. Acta* 2020, 187, 132–144.
11. Wang, H.; Pumera, M. Emerging materials for the fabrication of micro/nanomotors. *Nanoscale* 2017, 9, 2109–2116.
12. Sánchez, S.; Soler, L.; Katuri, J. Chemically Powered Micro- and Nanomotors. *Angew. Chem. Int. Ed.* 2015, 54, 1414–1444.
13. Yang, Q.; Xu, H.; Wen, H.; Zhao, H.; Liu, X.; Cai, Y.; Wang, H.; Dong, R. Graphene oxide induced enhancement of light-driven micromotor with biocompatible fuels. *Appl. Mater. Today* 2021, 22, 100943–1010036.
14. Dubal, D.P.; Chodankar, N.R.; Kim, D.-H.; Gomez-Romero, P. Towards flexible solid-state supercapacitors for smart and wearable electronics. *Chem. Soc. Rev.* 2018, 47, 2065–2129.
15. Liang, X.; Mou, F.; Huang, Z.; Zhang, J.; You, M.; Xu, L.; Luo, M.; Guan, J. Hierarchical Microswarms with Leader-Follower-Like Structures: Electrohydrodynamic Self-Organization and Multimode Collective Photoresponses. *Adv. Funct. Mater.* 2020, 30, 1908602–1908620.
16. Ge, Y.; Wang, T.; Zheng, M.; Jiang, Z.; Wang, S. Controlled one-sided growth of Janus TiO₂/MnO₂ nanomotors. *Nanotechnology* 2019, 30, 315702.
17. Wang, Y.; Li, Z.; Solovev, A.A.; Huang, G.; Mei, Y. Light-controlled two-dimensional TiO₂ plate micromotors. *RSC Adv.* 2019, 9, 29433–29439.
18. Chen, C.; Tang, S.; Teymourian, H.; Karshalev, E.; Zhang, F.; Li, J.; Mou, F.; Liang, Y.; Guan, J.; Wang, J. Chemical/Light-Powered Hybrid Micromotors with “On-the-Fly” Optical Brakes. *Angew. Chem. Int. Ed.* 2018, 57, 8110–8114.

19. Yu, T.; Athanassiadis, A.G.; Popescu, M.N.; Chikkadi, V.; Güth, A.; Singh, D.P.; Qiu, T.; Fischer, P. Microchannels with Self-Pumping Walls. *ACS Nano* 2020, 14, 13673–13680.
20. Feng, P.; Du, X.; Guo, J.; Wang, K.; Song, B. Light-Responsive Nanofibrous Motor with Simultaneously Precise Locomotion and Reversible Deformation. *ACS Appl. Mater. Interfaces* 2021, 13, 8985–8996.
21. Maghsoodi, A.; Bhattacharya, K. Light-induced swirling and locomotion. *Proc. R. Soc. A Math. Phys. Eng. Sci.* 2022, 478.
22. Lan, R.; Sun, J.; Shen, C.; Huang, R.; Zhang, Z.; Ma, C.; Bao, J.; Zhang, L.; Wang, L.; Yang, D.; et al. Light-Driven Liquid Crystalline Networks and Soft Actuators with Degree-of-Freedom-Controlled Molecular Motors. *Adv. Funct. Mater.* 2020, 30, 202000252.
23. Liras, M.; Barawi, M.; De La Peña O'Shea, V.A. Hybrid materials based on conjugated polymers and inorganic semiconductors as photocatalysts: From environmental to energy applications. *Chem. Soc. Rev.* 2019, 48, 5454–5487.
24. Li, W.; Wu, X.; Qin, H.; Zhao, Z.; Liu, H. Light-Driven and Light-Guided Microswimmers. *Adv. Funct. Mater.* 2016, 26, 3164–3171.
25. Pimienta, V.; Antoine, C. Self-propulsion on liquid surfaces. *Curr. Opin. Colloid Interface Sci.* 2014, 19, 290–299.
26. Kavokine, N.; Anyfantakis, M.; Morel, M.; Rudiuk, S.; Bickel, T.; Baigl, D. Light-Driven Transport of a Liquid Marble with and against Surface Flows. *Angew. Chem. Int. Ed.* 2016, 55, 11183–11187.
27. Sridhar, V.; Park, B.-W.; Sitti, M. Light-Driven Janus Hollow Mesoporous TiO₂-Au Microswimmers. *Adv. Funct. Mater.* 2018, 28, 1704902–1704932.
28. Wang, Q.-L.; Wang, C.; Dong, R.-F.; Pang, Q.-Q.; Cai, Y.-P. Steerable light-driven TiO₂-Fe Janus micromotor. *Inorg. Chem. Commun.* 2018, 91, 1–4.
29. Chen, B.; Ding, M.; Tan, H.; Wang, S.; Liu, L.; Wang, F.; Tian, H.; Gao, J.; Ye, Y.; Fu, D.; et al. Visible-light-driven TiO₂@N-Au nanorobot penetrating the vitreous. *Appl. Mater. Today* 2022, 27, 101455.
30. Tang, S.; Zhang, F.; Zhao, J.; Talaat, W.; Soto, F.; Karshalev, E.; Chen, C.; Hu, Z.; Lu, X.; Li, J.; et al. Structure-Dependent Optical Modulation of Propulsion and Collective Behavior of Acoustic/Light-Driven Hybrid Microbowls. *Adv. Funct. Mater.* 2019, 29, 1809003–1809019.
31. Wang, X.; Sridhar, V.; Guo, S.; Talebi, N.; Miguel-López, A.; Hahn, K.; van Aken, P.A.; Sánchez, S. Fuel-Free Nanocap-Like Motors Actuated Under Visible Light. *Adv. Funct. Mater.* 2018, 28, 1705862–1705899.
32. Wittmann, M.; Ali, A.; Gemming, T.; Stavale, F.; Simmchen, J. Semiconductor-Based Microswimmers: Attention to Detail Matters. *J. Phys. Chem. Lett.* 2021, 12, 9651–9656.
33. Lin, X.; Zhu, H.; Zhao, Z.; You, C.; Kong, Y.; Zhao, Y.; Liu, J.; Chen, H.; Shi, X.; Makarov, D.; et al. Hydrogel-Based Janus Micromotors Capped with Functional Nanoparticles for Environmental Applications. *Adv. Mater. Technol.* 2020, 5, 2000279–2000299.
34. Nicholls, D.; DeVerse, A.; Esplin, R.; Castañeda, J.; Loyd, Y.; Nair, R.; Voinescu, R.; Zhou, C.; Wang, W.; Gibbs, J.G. Shape-Dependent Motion of Structured Photoactive Microswimmers. *ACS Appl. Mater. Interfaces* 2018, 10, 18050–18056.
35. Holterhoff, A.L.; Li, M.; Gibbs, J.G. Self-Phoretic Microswimmers Propel at Speeds Dependent upon an Adjacent Surface's Physicochemical Properties. *J. Phys. Chem. Lett.* 2018, 9, 5023–5028.
36. Wang, L.; Popescu, M.N.; Stavale, F.; Ali, A.; Gemming, T.; Simmchen, J. Cu@TiO₂ Janus microswimmers with a versatile motion mechanism. *Soft Matter* 2018, 14, 6969–6973.
37. Dai, J.; Cheng, X.; Li, X.; Wang, Z.; Wang, Y.; Zheng, J.; Liu, J.; Chen, J.; Wu, C.; Tang, J. Solution-Synthesized Multifunctional Janus Nanotree Microswimmer. *Adv. Funct. Mater.* 2021, 31, 2106204.
38. Deng, Z.; Mou, F.; Tang, S.; Xu, L.; Luo, M.; Guan, J. Swarming and collective migration of micromotors under near infrared light. *Appl. Mater. Today* 2018, 13, 45–53.
39. Sridhar, V.; Park, B.-W.; Guo, S.; van Aken, P.A.; Sitti, M. Multiwavelength-Steerable Visible-Light-Driven Magnetic CoO–TiO₂ Microswimmers. *ACS Appl. Mater. Interfaces* 2020, 12, 24149–24155.
40. Maric, T.; Nasir, M.Z.M.; Webster, R.D.; Pumera, M. Tailoring Metal/TiO₂ Interface to Influence Motion of Light-Activated Janus Micromotors. *Adv. Funct. Mater.* 2020, 30, 1908614–1908629.
41. Duan, S.; Xu, P.; Wang, W. Better fuels for photocatalytic micromotors: A case study of triethanolamine. *Chem. Commun.* 2021, 57, 9902–9905.
42. Zhang, J.; Mou, F.; Tang, S.; Kauffman, J.E.; Sen, A.; Guan, J. Photochemical micromotor of eccentric core in isotropic hollow shell exhibiting multimodal motion behavior. *Appl. Mater. Today* 2022, 26, 101371.

43. Étude O'Neel-Judy, J.G.G.; Nicholls, D.; Castañeda, J.; Gibbs, J.G. Light-Activated, Multi-Semiconductor Hybrid Microswimmers. *Small* 2018, 14, e1801860.
44. Ikram, M.; Hu, F.; Peng, G.; Basharat, M.; Jabeen, N.; Pan, K.; Gao, Y. Light-Activated Fuel-Free Janus Metal Organic Framework Colloidal Motors for the Removal of Heavy Metal Ions. *ACS Appl. Mater. Interfaces* 2021, 13, 51799–51806.
45. Liu, M.; Jiang, J.; Tan, H.; Chen, B.; Ou, J.; Wang, H.; Sun, J.; Liu, L.; Wang, F.; Gao, J.; et al. Light-driven Au–ZnO nanorod motors for enhanced photocatalytic degradation of tetracycline. *Nanoscale* 2022, 14, 12804–12813.
46. He, X.; Jiang, H.; Li, J.; Ma, Y.; Fu, B.; Hu, C. Dipole-Moment Induced Phototaxis and Fuel-Free Propulsion of ZnO/Pt Janus Micromotors. *Small* 2021, 17, 2101388.
47. Zhan, X.; Zheng, J.; Zhao, Y.; Zhu, B.; Cheng, R.; Wang, J.; Liu, J.; Tang, J.; Tang, J. From Strong Dichroic Nanomotor to Polarotactic Microswimmer. *Adv. Mater.* 2019, 31, e1903329.
48. Pourrahimi, A.M.; Villa, K.; Ying, Y.; Sofer, Z.; Pumera, M. ZnO/ZnO₂/Pt Janus Micromotors Propulsion Mode Changes with Size and Interface Structure: Enhanced Nitroaromatic Explosives Degradation under Visible Light. *ACS Appl. Mater. Interfaces* 2018, 10, 42688–42697.
49. Ji, F.; Zhou, D.; Zhang, G.; Li, L. Numerical Analysis of Visible Light Driven Gold/Ferric Oxide Nanomotors. *IEEE Trans. Nanotechnol.* 2018, 17, 692–696.
50. Pourrahimi, A.M.; Villa, K.; Palenzuela, C.L.M.; Ying, Y.; Sofer, Z.; Pumera, M. Catalytic and Light-Driven ZnO/Pt Janus Nano/Micromotors: Switching of Motion Mechanism via Interface Roughness and Defect Tailoring at the Nanoscale. *Adv. Funct. Mater.* 2019, 29, 1808678–1808685.
51. Zhou, X.; Li, Z.; Tan, L.; Zhang, Y.; Jiao, Y. Near-Infrared Light-Steered Graphene Aerogel Micromotor with High Speed and Precise Navigation for Active Transport and Microassembly. *ACS Appl. Mater. Interfaces* 2020, 12, 23134–23144.
52. Maria-Hormigos, R.; Jurado-Sánchez, B.; Escarpa, A. Graphene quantum dot based micromotors: A size matter. *Chem. Commun.* 2019, 55, 6795–6798.
53. Wang, Q.; Dong, R.; Yang, Q.; Wang, J.; Xu, S.; Cai, Y. Highly efficient visible-light-driven oxygen-vacancy-based Cu₂+1O micromotors with biocompatible fuels. *Nanoscale Horiz.* 2020, 5, 325–330.
54. Chen, X.; Ding, X.; Liu, Y.; Li, J.; Liu, W.; Lu, X.; Gu, Z. Highly efficient visible-light-driven Cu₂O@CdSe micromotors adsorbent. *Appl. Mater. Today* 2021, 25, 101200.
55. Liu, W.; Chen, X.; Ding, X.; Long, Q.; Lu, X.; Wang, Q.; Gu, Z. Visible-light-driven cuprous oxide nanomotors with surface-heterojunction-induced propulsion. *Nanoscale Horiz.* 2021, 6, 238–244.
56. Chen, Z.; Jiang, J.; Wang, X.; Zhang, H.; Song, B.; Dong, B. Visible light-regulated BiVO₄-based micromotor with biomimetic 'predator-bait' behavior. *J. Mater. Sci.* 2022, 57, 4092–4103.
57. Villa, K.; Novotný, F.; Zelenka, J.; Browne, M.P.; Ruml, T.; Pumera, M. Visible-Light-Driven Single-Component BiVO₄ Micromotors with the Autonomous Ability for Capturing Microorganisms. *ACS Nano* 2019, 13, 8135–8145.
58. Kong, L.; Mayorga-Martinez, C.C.; Guan, J.; Pumera, M. Fuel-Free Light-Powered TiO₂/Pt Janus Micromotors for Enhanced Nitroaromatic Explosives Degradation. *ACS Appl. Mater. Interfaces* 2018, 10, 22427–22434.
59. Fu, S.; Fu, D.; Xie, D.; Liu, L.; Chen, B.; Ye, Y.; Wilson, D.A.; Peng, F. Light driven micromotor swarm for tumor photothermal therapy. *Appl. Mater. Today* 2022, 26, 101348.
60. Zhang, J.; Mou, F.; Wu, Z.; Tang, S.; Xie, H.; You, M.; Liang, X.; Xu, L.; Guan, J. Simple-Structured Micromotors Based on Inherent Asymmetry in Crystalline Phases: Design, Large-Scale Preparation, and Environmental Application. *ACS Appl. Mater. Interfaces* 2019, 11, 16639–16646.
61. Peng, X.; Urso, M.; Pumera, M. Metal oxide single-component light-powered micromotors for photocatalytic degradation of nitroaromatic pollutants. *npj Clean Water* 2023, 6, 1–7.
62. Hong, Y.; Diaz, M.; Córdova-Figueroa, U.M.; Sen, A. Light-Driven Titanium-Dioxide-Based Reversible Microfireworks and Micromotor/Micropump Systems. *Adv. Funct. Mater.* 2010, 20, 1568–1576.
63. Yu, T.; Chuphal, P.; Thakur, S.; Reigh, S.Y.; Singh, D.P.; Fischer, P. Chemical micromotors self-assemble and self-propel by spontaneous symmetry breaking. *Chem. Commun.* 2018, 54, 11933–11936.
64. She, P.; Qin, J.S.; Rao, H.; Guan, B.; Yu, J. Spatially separated bimetallic cocatalysts on hollow-structured TiO₂ for photocatalytic hydrogen generation. *Mater. Chem. Front.* 2020, 4, 1671–1678.
65. Zheng, J.; Dai, B.; Wang, J.; Xiong, Z.; Yang, Y.; Liu, J.; Zhan, X.; Wan, Z.; Tang, J. Orthogonal navigation of multiple visible-light-driven artificial microswimmers. *Nat. Commun.* 2017, 8, 1–7.

66. Jang, B.; Hong, A.; Kang, H.E.; Alcantara, C.; Charreyron, S.; Mushtaq, F.; Pellicer, E.; Büchel, R.; Sort, J.; Lee, S.S.; et al. Multiwavelength Light-Responsive Au/B-TiO₂ Janus Micromotors. *ACS Nano* 2017, 11, 6146–6154.
67. Pourrahimi, A.M.; Villa, K.; Sofer, Z.; Pumera, M. Light-Driven Sandwich ZnO/TiO₂/Pt Janus Micromotors: Schottky Barrier Suppression by Addition of TiO₂ Atomic Interface Layers into ZnO/Pt Micromachines Leading to Enhanced Fuel-Free Propulsion. *Small Methods* 2019, 3, 1900258.
68. Ke, H.; Ye, S.; Carroll, R.L.; Showalter, K. Motion Analysis of Self-Propelled Pt–Silica Particles in Hydrogen Peroxide Solutions. *J. Phys. Chem. A* 2010, 114, 5462–5467.
69. Mbayachi, V.B.; Ndayiragije, E.; Sammani, T.; Taj, S.; Mbuta, E.R.; Khan, A.U. Graphene synthesis, characterization and its applications: A review. *Results Chem.* 2021, 3, 100163.
70. Orozco, J.; Mercante, L.A.; Pol, R.; Merkoçi, A. Graphene-based Janus micromotors for the dynamic removal of pollutants. *J. Mater. Chem. A* 2016, 4, 3371–3378.
71. Mayorga-Martinez, C.C.; Vyskočil, J.; Novotný, F.; Pumera, M. Light-driven Ti₃C₂ MXene micromotors: Self-propelled autonomous machines for photodegradation of nitroaromatic explosives. *J. Mater. Chem. A* 2021, 9, 14904–14910.
72. Urso, M.; Ussia, M.; Novotný, F.; Pumera, M. Trapping and detecting nanoplastics by MXene-derived oxide microrobots. *Nat. Commun.* 2022, 13, 3573.
73. Urso, M.; Bruno, L.; Dattilo, S.; Carroccio, S.C.; Mirabella, S. Band Engineering versus Catalysis: Enhancing the Self-Propulsion of Light-Powered MXene-Derived Metal–TiO₂ Micromotors to Degrade Polymer Chains. *ACS Appl. Mater. Interfaces* 2023, 16, 1293–1307.

Retrieved from <https://encyclopedia.pub/entry/history/show/126830>